Stochastic effects at ripple formation processes in anisotropic systems with multiplicative noise

Dmitrii O. Kharchenko,* Vasyl O. Kharchenko, Irina O. Lysenko, and Sergei V. Kokhan
Institute of Applied Physics, National Academy of Sciences of Ukraine, 58 Petropavlovskaya Street, 40030 Sumy, Ukraine
(Received 13 May 2010; revised manuscript received 27 September 2010; published 6 December 2010)

We study pattern formation processes in anisotropic system governed by the Kuramoto-Sivashinsky equation with multiplicative noise as a generalization of the Bradley-Harper model for ripple formation induced by ion bombardment. For both linear and nonlinear systems we study noise-induced effects at ripple formation and discuss scaling behavior of the surface growth and roughness characteristics. It was found that the secondary parameters of the ion beam (beam profile and variations of an incidence angle) can crucially change the topology of patterns and the corresponding dynamics.

DOI: 10.1103/PhysRevE.82.061108 PACS number(s): 05.40.−a, 79.20.Rf, 68.35.Ct, 64.60.al

I. INTRODUCTION

Fabrication of nanoscale surface structures has attracted considerable attention due to their applications in electronics [1]. In the last five decades many studies have been devoted to understanding the mechanism of pattern formation and its control during ion-beam sputtering (see, for example, Refs. [2–9]). Among theoretical investigations there are a lot of experimental data manifesting a large class of patterns appeared as result of self-organization process on the surface of a solid. It was shown experimentally that main properties of pattern formation and structure of patterns depend on the energetic ion-beam parameters such as ion flux, energy of deposition, angle of incidence, and temperature. Formation of ripples was investigated on different substrates, i.e., on metals (Ag and Cu) [10,11], semiconductors (Ge [12] and Si [13–15]), Sn [16], InP [17], $Cd_2Nb_2O_7$ pyrochlore [18], and others. Height modulations on the surface induced by ion-beam sputtering result in formation of ripples having the typical size of $0.1-1$ μm and nanoscale patterns with the linear size of $35-250$ Å [19].

It is well known that orientation of ripples depends on the incidence angle. At the incidence angles around $\pi/2$ the wave vector of the modulations is parallel to the component of the ion beam in the surface plane, whereas at small incidence angles (close to grazing) the wave vector is perpendicular to this component. The orientation of ripples can be controlled by a penetration depth which is proportional to the deposited energy. Analytical investigations provided by Cuerno and Barabasi show a possible control of pattern formation governed by both the incidence angle and penetration depth [4,5]. The main theoretical models describing ripple formation are based on results of the famous works of Bradley and Harper [3], Kardar *et al.* [20], Wolf and Villian [21], and Kuramoto *et al.* [22]. The main mechanisms for pattern formation were set to predict orientation change of the ripples and formation of holes and dots. These models were generalized by taking into account additive fluctuations leading to statistical description of the corresponding processes.

Moreover, it was shown that under well-defined processing conditions the secondary ion-beam parameters (beam profile) may lead to different patterns [23]. Theoretical predictions including statistical properties of the beam profile were performed in Ref. [9]. It was shown that fluctuations in incident angles result in stochastic description of the ripple formation with multiplicative noise. Unfortunately, detailed description of pattern formation in such complicated stochastic systems was not discussed. Moreover, the problem of understanding the scaling behavior of the surface characteristics is still opened.

In this paper we aim to study ripple (or generally pattern) formation processes in anisotropic system governed by the corresponding Kuramoto-Sivashinsky equation which takes into account multiplicative noise caused by fluctuation of the incidence angle. We consider the linear and nonlinear models separately and discuss the corresponding phase diagrams in the space of main beam parameters reduced to the penetration depth and the angle of incidence. We present results of the scaling behavior study of the correlation functions and discuss time dependencies of the roughness and growth exponents during the system evolution as well as fractal properties of the surface. It will be shown that multiplicative fluctuations in ripple formation processes can accelerate surface modulations. We shall show that both phase diagrams and the scaling exponents crucially depend on the statistical properties of the beam.

The work is organized as follows. In Sec. II we present the stochastic model with multiplicative noise. Section III is devoted to the stability analysis of the linear system, where the main phase diagrams are discussed. The nonlinear stochastic model is studied in Sec. IV. Here, we consider the behavior of the main statistical characteristics of the surface such as distribution of the height field and scaling properties of the correlation functions. We summarize in Sec. V.

II. MODEL

Let us consider a d-dimensional substrate and denote with $\mathbf{r}$ the d-dimensional vector locating a point on it. The surface is described at each time t by the height $z=h(\mathbf{r},t)$. If we assume that the surface morphology is changed while ion sputtering, then we can use the model for the surface growth proposed by Bradley and Harper [3] and further developed by Cuerno and Barabasi [4]. We consider the system where the direction of the ion beam lies in the x-z plane at an angle

*dikh@ipfcentr.sumy.ua

θ from the normal of the uneroded surface. Following the standard approach one assumes that an averaged energy deposited at the surface (let say point O) due to the ion arriving at the point P in the solid follows the Gaussian distribution [3] $E(\mathbf{r})=[\epsilon/(2\pi)^{3/2}\sigma\mu^2]\exp[-z^2/2\sigma^2-(x^2+y^2)/2\mu^2]$; ϵ denotes the kinetic energy of the arriving ion, and σ and μ are the widths of the distribution in directions parallel and perpendicular to the incoming beam. Parameters σ and μ depend on the target material and can vary with physical properties of the target and incident energy. We consider the simplest case when $\sigma=\mu$. The erosion velocity at the surface point O is described by the formula $v=p\int_{\mathcal{R}}d\mathbf{r}\Phi(\mathbf{r})E(\mathbf{r})$, where integration is provided over the range of the energy distribution of all ions; here, $\Phi(\mathbf{r})$ and p are corrections for the local slope dependence of the uniform flux J and proportionality constant, respectively [24]. The general expression for the local flux for surfaces with nonzero local curvature is [25] $\Phi(x,y,h)=J\cos\{\arctan[\sqrt{(\nabla_x h)^2+(\nabla_y h)^2}]\}$. Hence, the dynamics of the surface height is defined by the relation $\partial_t h\simeq -v(\theta-\nabla_x h,\nabla_x^2 h,\nabla_y^2 h)$ and is given by the equation $\partial_t h\simeq -v(\theta)\sqrt{1+(\nabla h)^2}$, where $0<\theta<\pi/2$ [3–5,20,26]. The linear term expansion gives $\partial_t h=-v_0+\gamma\nabla_x h+\nu_\alpha\nabla_{\alpha\alpha}^2 h$, where $\nabla=\partial/\partial\mathbf{r}$, $\nabla_\alpha=\partial/\partial\alpha$, and $\alpha=\{x,y\}$. Here, v_0 is the surface erosion velocity, $\gamma=\gamma(\theta)$ is a constant that describes the slope depending erosion, and $\nu_\alpha=\nu_\alpha(\theta)$ is the effective surface tension generated by erosion process in the α direction.

If one assumes that the surface current is driven by differences in chemical potential μ, then the evolution equation for the field h should take into account the term $-\nabla\cdot\mathbf{j}_s$ in the right-hand side, where $\mathbf{j}_s=K\nabla(\nabla^2 h)$ is the surface current; $K>0$ is the temperature-dependent surface diffusion constant. If the surface diffusion is thermally activated, then we have $K=D_s\kappa\rho/n^2T$, where $D_s=D_0e^{-E_a/T}$ is the surface self-diffusivity (E_a is the activation energy for surface diffusion), κ is the surface free energy, ρ is the areal density of diffusing atoms, and n is the number of atoms per unit volume in the amorphous solid. This term in the dynamical equation for h is relevant in the high-temperature limit which will be studied below.

The quantities v_0, γ, and ν_α are functions of the angle θ only, not the temperature. Assuming that the surface varies smoothly, next we neglect spatial derivatives of the height h of third and higher orders in the slope expansion. Taking into account nonlinear terms in the slope expansion of the surface height dynamics, we arrive at the equation for the quantity $h'=h+v_0t$ of the form [3,4]

$$\partial_t h=\gamma\nabla_x h+\nu_\alpha\nabla_{\alpha\alpha}^2 h+\frac{\Lambda_\alpha}{2}(\nabla_\alpha h)^2-K\nabla^2(\nabla^2 h),\qquad(1)$$

where we drop the prime for convenience. Coefficients in Eq. (1) are defined in Ref. [4] and read

$$s=\sin\theta,\quad c=\cos\theta,\quad a_\sigma=a/\sigma,$$

$$F\equiv(\epsilon pJ/\sqrt{2\pi})\exp(-a_\sigma^2/2),$$

$$\gamma=\frac{F}{\sigma}s(a_\sigma^2c^2-1),$$

$$\Lambda_x=\frac{F}{\sigma}c[a_\sigma^2(3s^2-c^2)-a_\sigma^4s^2c^2],\quad \Lambda_y=-\frac{F}{\sigma}c(a_\sigma^2c^2),$$

$$\nu_x=\frac{F}{2}a_\sigma(2s^2-c^2-a_\sigma^2s^2c^2),\quad \nu_y=-\frac{F}{2}a_\sigma c^2.$$

Here, all control parameters are defined through the ion penetrate distance a, the incidence angle θ, the flux J, and the kinetic energy ϵ. It is known [25] that the penetration depth depends on the target material properties and the incoming ion energy ϵ: $a\approx\epsilon^{2m}/nC_m$, where n is the target atom density, C_m is the constant depending on the interatomic interaction potential [27], and $m\approx 1/2$ for intermediate energies (from 1 to 100 keV). Equation (1) is known as the noiseless anisotropic Kuramoto-Sivashinsky equation [22].

It was shown [3] that the linearized dynamical Eq. (1) admits a solution of the form $h(x,y,t)=A\exp[i(k_xx+k_yy-\omega t)+\varkappa t]$, where $\omega=-\gamma(\theta)k_x$ is the frequency and $\varkappa=-[\nu_x(\theta)k_x^2+\nu_y(\theta)k_y^2]-K(k_x^2+k_y^2)^2$ is the parameter responsible for a stability of the solution. During the system evolution a selection of wave numbers responsible for ripple orientation occurs. The selected wave number is $k_\alpha^2=|\nu_\alpha|/2K$, where α refers to the direction (x or y) along which the associated ν_α has a smaller value.

For the noiseless nonlinear model (1) it was shown that as the sets ν_α and Λ_α are functions of the angle of incidence $\theta\in[0,\pi/2]$, there are three domains in the phase diagram (a_σ,θ), where ν_x and Λ_x change their signs separately [4]. It results in ripple formation in different directions x and y varying a_σ or θ.

To describe an evolution of the surface in more realistic conditions one should take into account that the bombarding ions reach the surface stochastically, i.e., at random position and time; generally, it can reach the surface at random angle lying in the vicinity of the angle incidence θ. Most of the models proposed to describe ripple formation due to the ion sputtering process incorporate additive fluctuations that take into account stochastic nature of arriving ions (see, for example, Refs. [4,6,14]). From the mathematical viewpoint such a stochastic source results in spreading the patterns and makes possible statistical description of the system. If this term is assumed as a Gaussian white noise in time and space, it cannot change the system behavior crucially [28,29].

If one supposes that the ion beam is composed of ions distributed with different incidence angles, then we have three possible cases [9]: (i) homogeneous beam when the erosion velocity depends on random ion-beam parameters and the average velocity is defined through the distribution function over beam directions, (ii) temporally fluctuating homogenous beam when the direction of illumination constitutes a stationary temporally homogeneous stochastic process, and (iii) spatiotemporally fluctuating beam when the directions of ions form a homogeneous and stationary field. In Ref. [9] the authors considered case (iii) under the assumption of Gaussian distribution of a beam profile centered at a fixed angle θ_0. Such a model means that the fluctuation term that can appear in the dynamical equation for the field h is some kind of a multiplicative noise (with intensity depending on the field h). Unfortunately only general perspectives

were reported for the nonlinear model, while main results relate to studying the linear model behavior. From the naive consideration one can expect that the multiplicative noise can qualitatively influence the dynamics of ripple formation in the nonlinear system.

In present paper we aim to consider the general problem of the ripple formation under the assumption of Gaussian distribution of the beam profile around θ_0 in the framework of the model given by Eq. (1) following the approach proposed in Ref. [9]. To describe the model we start from Eq. (1) which can be rewritten in the form $\partial_t h = f(\theta, \nabla_\alpha h)$, where f is a deterministic force. Considering small deviations from the fixed angle θ_0 we can expand the function $f(\theta, \nabla_\alpha h)$ in the vicinity of θ_0. Therefore, for the right-hand side we get $f = f_0 + (\partial f/\partial\theta)|_{\theta=\theta_0}\delta\theta$ and assume that $\delta\theta$ is a stochastic field, i.e., $\delta\theta = \delta\theta(\mathbf{r}, t)$. Assuming Gaussian properties for the stochastic component $\delta\theta$, we set

$$\langle \delta\theta(\mathbf{r},t)\rangle = 0, \quad \langle \delta\theta(\mathbf{r},t)\delta\theta(\mathbf{r}',t')\rangle = 2D\Sigma C_r(\mathbf{r}-\mathbf{r}')C_t(t-t'), \tag{2}$$

where D is the parameter depending on the beam characteristics such as J, ϵ, p, a, and σ; Σ is the noise intensity characterizing the dispersion of $\delta\theta$; and C_r and C_t are spatial and temporal correlation functions of the noise $\delta\theta$. In further consideration we assume that $\delta\theta$ is the quasi-white-noise in time with $C_t(t-t') \to \delta(t-t')$ and colored in space, i.e., $C_r(\mathbf{r}-\mathbf{r}') = (\sqrt{2\pi r_c^2})^{-d}\exp[-(\mathbf{r}-\mathbf{r}')^2/2r_c^2]$, where r_c is the correlation radius of fluctuations. At $\Sigma = 0$ no fluctuations in the beam directions (incidence angle) are realized (pure deterministic case).

Therefore, expanding coefficients at spatial derivatives in Eq. (1) we arrive at the Langevin equation of the form

$$\partial_t h = \gamma_0 \nabla_x h + \nu_{\alpha 0}\nabla^2_{\alpha\alpha} h + \frac{\Lambda_{\alpha 0}}{2}(\nabla_\alpha h)^2 - K\nabla^2(\nabla^2 h) + \left[\gamma_1 \nabla_x h + \nu_{\alpha 1}\nabla^2_{\alpha\alpha} h + \frac{\Lambda_{\alpha 1}}{2}(\nabla_\alpha h)^2\right]\delta\theta, \tag{3}$$

where $\gamma_0 = \gamma(\theta_0)$, $\nu_{\alpha 0} = \nu_\alpha(\theta_0)$, $\Lambda_{\alpha 0} = \Lambda_\alpha(\theta_0)$, $\gamma_1 = \partial_\theta\gamma|_{\theta=\theta_0}$, $\nu_{\alpha 1} = \partial_\theta\nu_\alpha|_{\theta=\theta_0}$, and $\Lambda_{\alpha 1} = \partial_\theta\Lambda_\alpha|_{\theta=\theta_0}$. The parameter D is reduced to the constant F, which means that multiplicative fluctuations appear only if the system is subjected to ion beam with $F \neq 0$. Therefore, the stochastic system is described by the anisotropic Kuramoto-Sivashinsky equation with the multiplicative noise.

III. STABILITY ANALYSIS OF THE LINEAR MODEL

It is known that transitions between two macroscopic phases in a given system occur due to the loss of stability of the state for the certain values of the control parameters. In the case of stochastic systems the linear stability analysis needs to be performed on a statistical moment of the perturbed state. We will now perform the stability analysis for the system with multiplicative fluctuations. To that end we average the Langevin equation (3) over noise and obtain

$$\partial_t\langle h\rangle = \gamma_0\nabla_x\langle h\rangle + \nu_{\alpha 0}\nabla^2_{\alpha\alpha}\langle h\rangle + \frac{\Lambda_{\alpha 0}}{2}\langle(\nabla_\alpha h)^2\rangle - K\nabla^2(\nabla^2\langle h\rangle) + \left\langle\left[\gamma_1\nabla_x h + \nu_{\alpha 1}\nabla^2_{\alpha\alpha} h + \frac{\Lambda_{\alpha 1}}{2}(\nabla_\alpha h)^2\right]\delta\theta\right\rangle. \tag{4}$$

The last term can be calculated using the Novikov theorem [30]. From a formal representation one has

$$\langle \mathcal{R}\,\delta\theta(x,y;t)\rangle = \int dt' \int dx' \int dy' \langle \delta\theta(x,y;t)\delta\theta(x',y';t')\rangle \times \left\langle \frac{\delta\mathcal{R}}{\delta(\delta\theta(x'y';t'))}\right\rangle, \tag{5}$$

where $\mathcal{R}$ is the functional, $\delta/\delta(\delta\theta)$ is the variational derivative. The integration is carried out over the whole range of x', y', and t'. For our model one has $\mathcal{R} = \gamma_1\nabla_x h + \nu_{\alpha 1}\nabla^2_{\alpha\alpha} h + (\Lambda_{\alpha 1}/2)(\nabla_\alpha h)^2$. The variational derivative can be computed with the help of the relation $\frac{\delta\mathcal{R}}{\delta(\delta\theta)} = \frac{\partial\mathcal{R}}{\partial h}\left(\frac{\partial h}{\partial\delta\theta}\right)_{\alpha=\alpha'}$, where the second term is obtained from the formal solution of the Langevin equation (3). It follows that the response function takes the form

$$\left(\frac{\partial h}{\partial\,\delta\theta}\right)_{\alpha=\alpha'} = \gamma_1\nabla_x h\,\delta(x-x') + \delta(\alpha-\alpha')\left\{\nu_{\alpha 1}\nabla^2_{\alpha\alpha} h + \frac{\Lambda_{\alpha 1}}{2}(\nabla_\alpha h)^2\right\}. \tag{6}$$

As a result the variational derivative can be written as follows:

$$\frac{\delta\mathcal{R}}{\delta(\delta\theta)} = \gamma_1\nabla_x\left\{\gamma_1\nabla_x h\,\delta(x-x') + \delta(\alpha-\alpha')\left[\nu_{\alpha 1}\nabla^2_{\alpha\alpha} h + \frac{\Lambda_{\alpha 1}}{2}(\nabla_\alpha h)^2\right]\right\} + \nu_{\alpha 1}\nabla^2_{\alpha\alpha}\left\{\gamma_1\nabla_x h\,\delta(x-x') + \delta(\beta-\beta')\left[\nu_{\beta 1}\nabla^2_{\beta\beta'} h + \frac{\Lambda_{\beta 1}}{2}(\nabla_\beta h)^2\right]\right\} + \Lambda_{\alpha 1}(\nabla_\alpha h)\nabla_\alpha\left\{\gamma_1\nabla_x h\,\delta(x-x') + \delta(\beta-\beta')\left[\nu_{\beta 1}\nabla^2_{\beta\beta'} h + \frac{\Lambda_{\beta 1}}{2}(\nabla_\beta h)^2\right]\right\}. \tag{7}$$

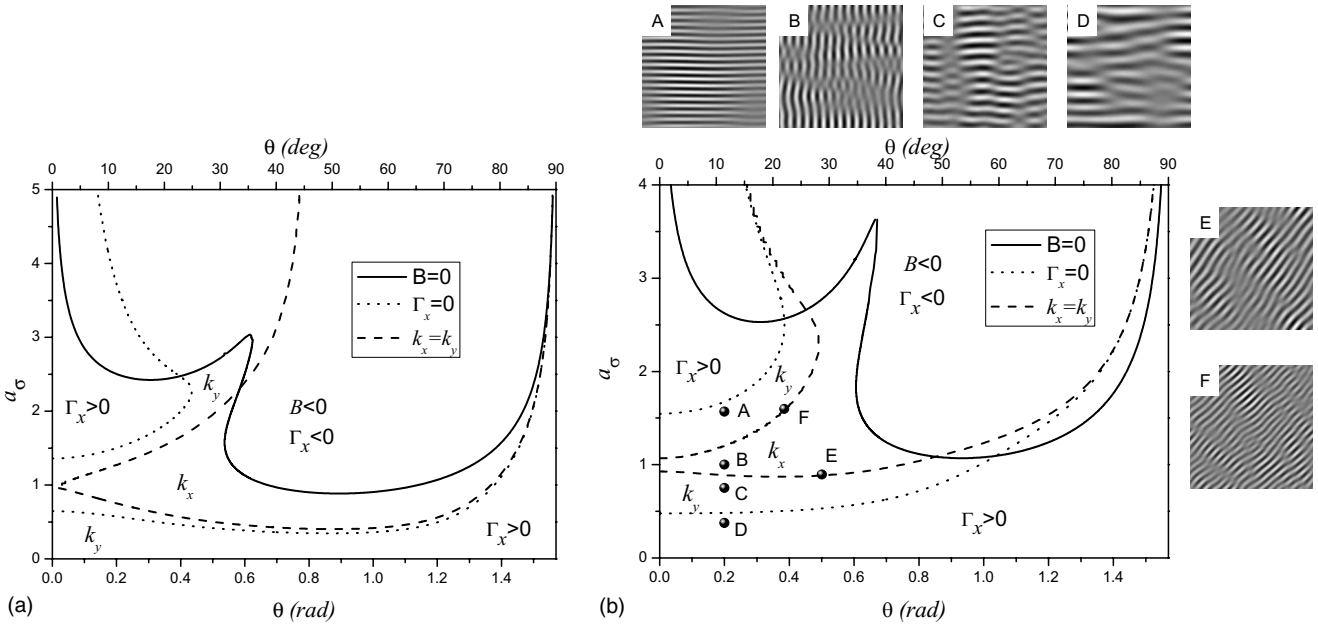

FIG. 1. Phase diagrams for the pattern selection at in the system with multiplicative noise with $\Sigma=1$ [in domains denoted with k_α where $\alpha\in\{x,y\}$ patterns with wave vector $\mathbf{k}=|k_\alpha|\hat{\alpha}$ are selected; plots (a) and (b) correspond to $r_c=0.65$ and $r_c=1$, respectively].

Let us consider the stability of the linear system. From the relation obtained it follows that terms with coefficients $\Lambda_{\alpha 1}$ lead to the nonlinear contribution, and hence can be neglected at this stage. Therefore, the reduced expression is of the form

$$\frac{\delta\mathcal{R}}{\delta(\delta\theta)} = \gamma_1^2\nabla_x[\nabla_x h\,\delta(x-x')] + \gamma_1\nu_{\alpha 1}\{\nabla_x[\nabla_{\alpha\alpha}^2 h\,\delta(\alpha-\alpha')] + \nabla_{\alpha\alpha}^2[\nabla_x h\,\delta(x-x')]\} + \nu_{\alpha 1}\nu_{\beta 1}\nabla_{\alpha\alpha}^2[\nabla_{\beta\beta}^2 h\,\delta(\alpha-\beta')]. \quad (8)$$

To perform next calculations we assume that the spatial correlation function for fluctuations can be decomposed as $C_r(\mathbf{r})=C_x(x)C_y(y)$ with maximum at $\alpha=\alpha'$, where $C(0)\equiv C_x(0)=C_y(0)$ and $C''|_{\alpha=\alpha'}\equiv\partial_{xx}^2 C_x|_{x=x'}=\partial_{yy}^2 C_y|_{y=y'}$, with $C''|_{\alpha=\alpha'}<0$. Then, integrating over t', and x' and y' (by parts), we obtain the expression for the decomposed correlator up to the first-order terms in h:

$$\langle[\gamma_1\nabla_x h + \nu_{\alpha 1}\nabla_{\alpha\alpha}^2 h + (\Lambda_{\alpha 1}/2)(\nabla_\alpha h)^2]\delta\theta\rangle = \{\nu_{\alpha 1}^2 C''|_{\alpha=\alpha'}\nabla_{\alpha\alpha}^2 + \gamma_1^2 C(0)\nabla_{xx}^2 + C(0)(\nu_{\alpha 1}\nabla_{\alpha\alpha}^2)^2 + \gamma_1\nu_{1x}[C''|_{\alpha=\alpha'}\nabla_x + C(0)\nabla_{xxx}^3] + \gamma_1\nu_{\alpha 1}C(0)\nabla_{\alpha\alpha}^2\nabla_x\}\langle h\rangle, \quad (9)$$

where only first-order terms in h are included.

Finally, we can rewrite the linearized evolution equation for the average $\langle h\rangle$ in the standard form

$$\partial_t\langle h\rangle = \widehat{\gamma_{ef}}\langle h\rangle + \widehat{\nu_{ef}}\langle h\rangle - \widehat{K_{ef}}\langle h\rangle, \quad (10)$$

where the following notation is used:

$$\widehat{\gamma_{ef}} \equiv \{\gamma_0 + \gamma_1\Sigma[\nu_{x1}C''|_{\alpha=\alpha'} + \nu_{x1}C(0)\nabla_{xx}^2 + \nu_{\alpha 1}C(0)\nabla_{\alpha\alpha}^2]\}\nabla_x,$$

$$\widehat{\nu_{ef}} \equiv (\nu_{\alpha 0} + \Sigma C''|_{\alpha=\alpha'}\nu_{\alpha 1}^2)\nabla_{\alpha\alpha}^2 + \gamma_1^2\Sigma C(0)\nabla_{xx}^2,$$

$$\widehat{K_{ef}} \equiv -K(\nabla_{\alpha\alpha}^2)^2 + \Sigma C(0)(\nu_{\alpha 1}\nabla_{\alpha\alpha}^2)^2. \quad (11)$$

It is easy to see that Eq. (10) admits a solution of the form $\langle h\rangle=A\exp[i(k_x x+k_y y-\omega t)+\varkappa t]$. Indeed, substituting it into Eq. (10) and separating real and imaginary parts we get

$$\omega = -k_x(\gamma_0 + \gamma_1\nu_{x1}\Sigma C''|_{x=x'}) + k_x\gamma_1\nu_{x1}\Sigma C(0)(k_x^2+k_y^2),$$

$$\varkappa = -k_x^2\Gamma_x - k_y^2\Gamma_y - K(k_x^2+k_y^2)^2 + \Sigma C(0)(\nu_{x1}^2k_x^2 + \nu_{y1}^2k_y^2)^2,$$

$$\Gamma_x \equiv \nu_{x0} + \nu_{x1}^2\Sigma C''|_{x=x'} + \gamma_1^2\Sigma C(0), \quad \Gamma_y \equiv \nu_{y0} + \nu_{y1}^2\Sigma C''|_{y=y'}. \quad (12)$$

It follows that if $\Gamma_\alpha<0$, then there will be a range of low frequencies that will grow exponentially. From our model one can see that as $\nu_{y0}<0$ and $C''<0$ with $C(0)>0$ the quantity Γ_y is always negative. Therefore, instability along the y direction will always appear. The quantity Γ_x can change sign as control parameters θ and a_σ and noise characteristics vary. It means that instability in the x direction can appear at the same incidence angles and penetration depths on one hand. On the other hand, the statistical characteristics of the noise reduced to the spatial correlation length r_c and the intensity Σ can change the system behavior drastically.

Stability change of the anisotropic system with an additive noise was discussed earlier [4]. Let us consider stability change in the system with the multiplicative noise. In Figs. 1(a) and 1(b) we plot the corresponding phase diagrams at fixed noise intensity Σ and different correlation radii r_c. Here, dotted lines limit domains of the stability of the system

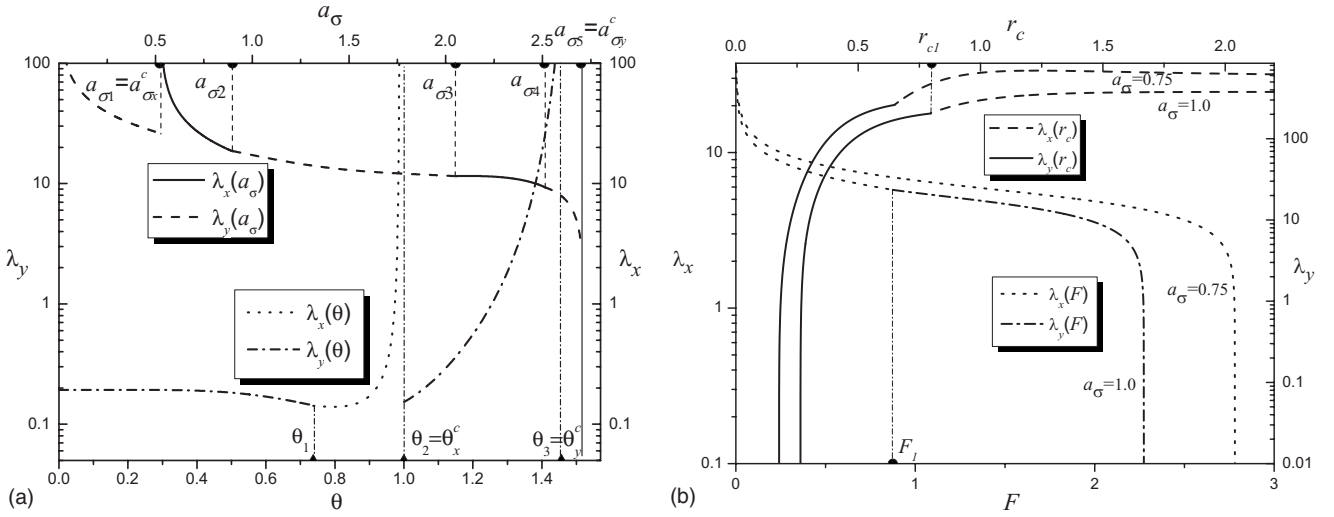

FIG. 2. (a) Plot of selected wavelengths λ_x and λ_y vs incidence angle θ at $a_\sigma=0.45$, $r_c=0.65$, and dimensionless penetration depth a_σ at $\theta=0.4763$ and $r_c=1.0$ ($a_{\sigma i}$, with $i\in 1,\ldots,4$ denoting threshold values when a change in the wave vector of patterns occurs); here, $0<\theta<\pi/2$ is measured in radians; other parameters are $F=1$ and $\sigma=1$. (b) Plot of selected wavelengths λ_x and λ_y vs the correlation scale r_c at $F=1.0$ and the energetic parameter F at $r_c=1.0$ at $\theta=0.4763$. Other parameters are $F=1$, $\sigma=1$, and $\Sigma=1$.

at low frequencies and relate to the case $\Gamma_x=0$. Solid line divides the space of a_σ and θ where the parameter $B\equiv 2K-4\Sigma C(0)\nu^4_{\alpha 1}$ takes zero values at $k_x=k_y$. This parameter is responsible for the stability of the system at large wave numbers. It is known that observable and selected ripples correspond to wave numbers with $k^2_\alpha=|\Gamma|/B$, where $B>0$ and $\Gamma=\min[\Gamma_x,\Gamma_y]$. Dashed lines in Fig. 1 correspond to the system parameters where $k_x=k_y$. In domains denoted with the corresponding wave number k_x or k_y ripples have the orientation in the x or y direction, respectively. As it follows from our linear stability analysis, orientation of ripples can be controlled varying both the penetration depth a_σ and the angle of incidence θ at fixed Σ and r_c. Comparing plots in Figs. 1(a) and 1(b) one can see that the statistical properties of the noise $\delta\theta$ are responsible for the change in the system behavior. Indeed, at small correlation radius of the angle fluctuations the domain of the system instability at fixed $a_\sigma=1$ is bigger than at large r_c. Moreover, the variation of quantity r_c can lead to a decrease in the system parameters where ripples oriented along k_x are observed. It is interesting to note that at large r_c at fixed interval of the angles of incidence θ a reorientation of ripples can be found varying parameter a_σ related to the deposited energy of the beam. Indeed, in the interval of θ lying between the abscissa of point E and abscissa of point F some kind of re-entrance is observable: at small a_σ (below the bottom dashed line where $k_x=k_y$) the ripples are oriented along k_y; in the intermediate domain of a_σ (between two dashed lines) the ripples are oriented along k_x; at large a_σ the ripples are oriented along k_y again (see snapshots for points $A-D$). The same situation is realized at fixed a_σ when the angle of incidence varies. For the system parameters related to the dashed lines (see points E and F) the ripples are characterized by $k_y=k_y$ with the orientation angle $\pi/4$.

Next, we calculate the selected wavelengths λ_x and λ_y versus the angle of incidence θ and the penetration depth a_σ [Fig. 2(a)] and versus the correlation scale r_c and the energetic parameter F [Fig. 2(b)]. The selected wavelengths relate to the smallest wave number in the corresponding direction. It is seen that as a_σ or θ varies transformations in ripple orientation occur. Here, $a_{\sigma i}$ and θ_i are threshold magnitudes for the penetration depth and incidence angle, respectively, indicating change in the ripple orientation. It is seen that there are two critical values $a_{\sigma 1}=a^c_{\sigma x}$ and $a_{\sigma 5}=a^c_{\sigma y}$ where the corresponding wavelengths take infinitely large magnitudes due to $\Gamma_x=0$. There are two critical values for the angle, $\theta_2=\theta^c_x$ and $\theta_3=\theta^c_y$, indicating divergence of the wavelengths when Γ_x takes zero values. From Fig. 2(b) one can see that as the energetic parameter F increases the wavelength of the ripple formation reduces to zero. At small a_σ the orientation of selected ripples can be changed at $F=F_1$, whereas at large values for the penetration depth no change is possible in the ripple orientation. The dependencies $\lambda_\alpha(r_c)$ manifest nonmonotonic behavior: at small r_c the wavelength increases, whereas at large r_c the decreasing dependencies are observed. Moreover, there is a critical value for the correlation radius r_{c1} where the orientation of ripples can be changed. Therefore, correlation properties of the ion beam can play a crucial role in ripple formation processes at early stages (in linear models). From the equations obtained for the selected wave numbers it follows that the selected wavelengths have the well-known asymptotics versus main parameters of the beam [$\lambda\sim T^{-1/2}\exp(-E_a/T)$, $\lambda\sim\epsilon^{-1/2}$, and $\lambda\sim J^{-1/2}$] and depend asymptotically versus secondary characteristics: $\lambda\sim(\mathcal{C}_\Sigma-\Sigma)^{1/2}$ and $\lambda\sim(\mathcal{C}_{r_c}-r_c)^{-1}$, where $\mathcal{C}_\Sigma$ and $\mathcal{C}_{r_c}$ are constants depending on the main system parameters. As it follows from Fig. 2(b) at $r_c\to\mathcal{C}_{r_c}$ the selected wavelength $\lambda_y(r_c)$ abruptly goes to zero (see solid curve).

IV. NONLINEAR STOCHASTIC MODEL

Next, let us consider the nonlinear system behavior setting $\Lambda_\alpha\neq 0$. In further study we are based on the simulation procedure allowing us to solve the nonlinear stochastic dif-

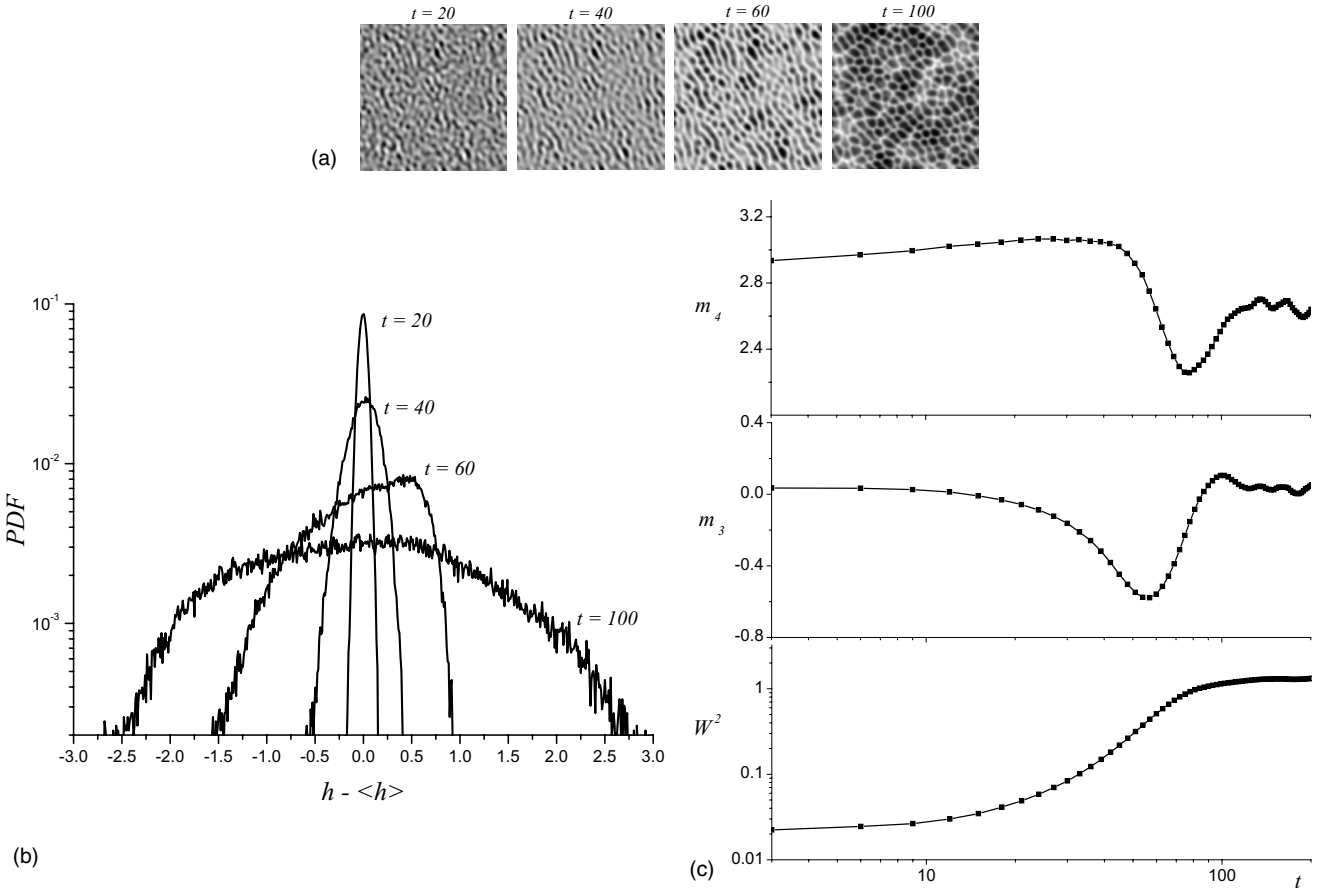

FIG. 3. A typical evolution of the system with multiplicative fluctuations at early stages. (a) Snapshots of images of the field h distribution for various growth times (dark color indicates low h, while white areas relate to high h). (b) Probability density function of the height for various growth times. (c) Kurtosis, skewness, and interface width versus growth time. Other parameters are $a_\sigma=1.2$, $\theta=0.4$, $F=1.0$, $\sigma=1.0$, $K=2.0$, $\Sigma=1.0$, and $r_c=1.0$.

ferential equation (3). As it was done in the previous section we use the finite-difference approach to calculate the evolution of the field h.

A. Evolution of the height distribution function

To investigate properties of a distribution of the field h we use skewness m_3 and kurtosis m_4, defined as

$$m_3 = \frac{\langle [h(\mathbf{r}) - \langle h(\mathbf{r})\rangle]^3\rangle}{W^3},$$

$$m_4 = \frac{\langle [h(\mathbf{r}) - \langle h(\mathbf{r})\rangle]^4\rangle}{W^4},$$

$$W^2 = \langle [h(\mathbf{r}) - \langle h(\mathbf{r})\rangle]^2\rangle, \tag{13}$$

where $\langle h(\mathbf{r})\rangle$ is the average of the height field [$\langle h(\mathbf{r})\rangle \equiv V^{-1}\Sigma_{\mathbf{r}} h(\mathbf{r},t)$, where $V=L^d$ is the system volume, with d as the spatial dimension and L as the linear size of the system] and W is the interface width. Skewness is a measure of the symmetry of a profile about the reference surface level. Its sign tells whether the father points are proportionately above ($m_3>0$) or below ($m_3<0$) the average surface level. Kurtosis describes randomness of the surface relative to that of a perfectly random (Gaussian) surface; for the Gaussian distribution one has $m_4=3.0$. Kurtosis is a measure of the sharpness of the height distribution function. It is known that if most of the surface features are concentrated near the mean surface level, then the kurtosis will be less than that if the height distribution contained a larger portion of the surface features lying farther from the mean surface level.

To solve the multiplicative noise Langevin equation treated in the Stratonovich sense we use the Milstein scheme [31]. The white noise source was generated with the help of the Box-Muller algorithm, satisfying generation of random numbers with the Gaussian distribution [32]. Simulations were provided on quadratic lattice $L\times L$ of the linear size $L=256$ with periodic boundary conditions. Spatial derivatives of the second and fourth orders were computed according to the standard finite-difference scheme; the nonlinear term $(\nabla h)^2$ was computed according to the scheme proposed in Refs. [33,34]. We have used Gaussian initial conditions taking $\langle h(\mathbf{r},t=0)\rangle=0$ and $\langle(\delta h)^2\rangle=0.1$; the integration time step is $\Delta t=0.005$ and the space step is $\ell=1$. All measured quantities were averaged over 20 independent realizations.

Figure 3(a) shows snapshots of the surface morphology for the set of parameters $a_\sigma=1.2$, $\theta=0.4$, $F=1.0$, $\sigma=1.0$,

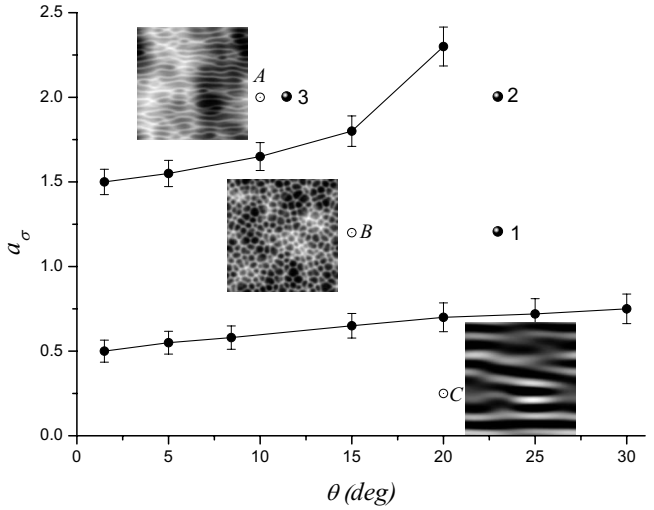

FIG. 4. Phase diagram for the anisotropic nonlinear model at $F=1$, $\sigma=1$, $\Sigma=1$, and $r_c=1$. Snapshots are taken at the system parameters related to position of the points A, B, and C, respectively.

$K=2.0$, $\Sigma=1.0$, and $r_c=1.0$ at $t=20$, 40, 60, and 100, respectively. It is seen that with an increase in the growth time, the lateral length of the surface features becomes bigger and holes (black regions) are formed at $t=100$. It follows that due to nonlinear effects and noise action the surface morphology is crucially changed comparing to the ripples shown in Fig. 1(b). Figure 3(b) illustrates the corresponding height probability density distribution function of these surfaces. It is seen that at $t=20$ the distribution is close to the Gaussian distribution. With the time growth one gets a deviation from zero-centered Gaussian distribution; after transient period of time the probability density function becomes symmetrical and centered at zero. In Fig. 3(c) we plot the kurtosis m_4, the skewness m_3, and the interface width W as functions of the growth time for above system parameters. According to initial conditions we have $m_4 \simeq 3.0$, $m_3 \simeq 0$, and $W \simeq 0$ at $t \simeq 0$. With the increase in the growth time the kurtosis grows until maximum is reached. The skewness decreases to its minimum and tends to zero after. These two quantities reflect the form of the distribution function shown in Fig. 3(b). The interface width increases algebraically toward a saturation regime at large t.

We have computed phase diagram for the nonlinear systems illustrating formation of different patterns shown in Fig. 4. It is seen that the numerical results are well related to analytical predictions from the linear stability analysis. Indeed, critical points lying on the lines correspond to a change in the quantity Γ_x. At large and low penetration depth a_σ ripples oriented along k_y direction are observed (see snapshot for the point C) due to $\Gamma_x > 0$. At the intermediate values of a_σ random patterns (holes) are realized due to the nonlinear influence of both the deterministic term $\Lambda_\alpha(\nabla_\alpha h)^2$ and the stochastic contribution.

B. Scaling properties of the surface morphology

Using numerical data it is possible to study statistical properties of the system considering the time-dependent height-height correlation function, determined as follows: $C_h(\mathbf{r},t)=\langle[h(\mathbf{r}+\mathbf{r}',t)-h(\mathbf{r}',t)]^2\rangle$. In the framework of dynamic scaling hypothesis one can write the correlation function in the form [35,36]

$$C_h(\mathbf{r},t) = 2W^2(t)\phi\left(\frac{r}{\xi(t)}\right), \tag{14}$$

where

$$\phi(u) \sim \begin{cases} u^{2\alpha}, & \text{for } u \ll 1 \\ \text{const}, & \text{for } u \gg 1. \end{cases} \tag{15}$$

Early stages can be fitted by the function [37] $C_h(\mathbf{r},t) \approx 2W^2(t)\{1-\exp[-(r/\xi)^{2\alpha}]\}$. The dynamic scaling hypothesis assumes that the following dependencies hold: $W^2(t) \propto t^{2\beta}$ and $\xi(t) \propto t^{1/z}$, where β is the growth exponent and z is the dynamic exponent for which $z=\alpha/\beta$. From another viewpoint one can assume [34]

$$C_h(\mathbf{r},t) = r^{2\alpha}\psi\left(\frac{t}{r^z}\right), \tag{16}$$

where

$$\psi(v) \sim \begin{cases} v^{2\beta}, & \text{for } v \ll 1 \\ \text{const}, & \text{for } v \gg 1, \end{cases} \tag{17}$$

and the relation $z=\alpha/\beta$ holds. Therefore, these two cases lead to the same results $C_h(t) \propto t^{2\beta}$ and $C_h(r) \propto r^{2\alpha}$, allowing one to define the growth exponent β and the roughness exponent α. As was shown in Ref. [34] the roughness $W(t,L)$ can be related to the structure function $S(\mathbf{k})$ as follows: $W^2(t,L)=V^{-1}\Sigma_{\mathbf{k}\neq 0}S(\mathbf{k},t)$, where $S_h(k,t)=V^{-1}\langle h_k(t)h_{-k}(t)\rangle$. The structure function $S(k,t)$ has the form

$$S_h(k,t) = k^{-(d+2\alpha)}\Theta(k^z t), \tag{18}$$

where

$$\Theta(k^z t) \sim \begin{cases} k^{2\alpha}t^{2\alpha/\beta}, & \text{for } k^z t \ll 1 \\ \text{const}, & \text{for } k^z t \gg 1, \end{cases} \tag{19}$$

and scales as $S_h(k,t) \propto k^{-(d+2\alpha)}$ for large t and $S_h(k,t) \propto t^{2\beta}$ for small t.

In previous studies (see, for example, Ref. [6]) it was shown that even in the isotropic system with additive noise scaling exponents α, β, and z depend on the system parameters ν_0, Λ_0, and K. Moreover, these exponents are the time-dependent functions, i.e., its magnitudes can be changed in the course of the system evolution.

In our study we have taken into account multiplicative noise described by the energetic characteristics of the beam and additionally by the noise intensity Σ and correlation radius of fluctuations r_c. Therefore, one should expect that due to renormalization of the main system parameters responsible for the stability of the system and nonlinear effects in its behavior, such scaling exponents are functions of the above noise properties. To prove it we compare magnitudes of both scaling exponents α and β for the system with additive fluctuations and for the system with our multiplicative noise.

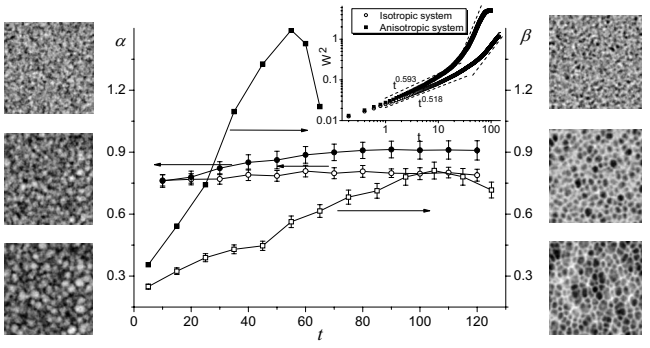

FIG. 5. Roughness exponent α and growth exponent β versus growth time for isotropic Kuramoto-Sivashinsky equation with additive noise (white circles and squares) at $\nu_x=\nu_y=-0.2$, $\Lambda_x=\Lambda_y=1.0$, $K=2$ and anisotropic Kuramoto-Sivashinsky equation with additive noise (black circles and squares) at $a_\sigma=1.2$, $\theta=0.4$, $K=2$. Snapshots are shown for above two models (left for isotropic and right for anisotropic Kuramoto-Sivashinsky equation with additive noise) at $t=20$, 60, and 100 from top to bottom. The noise intensity $\Sigma=1.0$.

To characterize fractal properties of the surface one can study a pair-correlation function defined as follows:

$$C_p(\mathbf{r};t)=\langle h(\mathbf{r}+\mathbf{r}';t)h(\mathbf{r};t)\rangle. \tag{20}$$

If there is no characteristic space scale, then the introduced correlation function should behave itself algebraically, i.e., $C_p(r;t)\propto 1/r^{\Delta}$, where the scaling exponent Δ relates to the fractal correlation dimension D_2 as $\Delta=d-D_2$. The corresponding Fourier transformation of the correlation function $C_p(\mathbf{r};t)$ scales as $S_p(k;t)\propto k^{-D_2}$. From the definition of the correlation fractal dimension D_2 and the properties of the Fourier component of correlator (20) it follows that at $D_2=0$ there is no scaling behavior of the structure function and $S_p(k;t)\approx$ const. Hence, the surface at the fixed time t can be considered as a Gaussian surface with no correlation, i.e., white noise in space with equal contribution of all wave numbers k; the corresponding spatial correlator (20) is reduced to the Dirac delta function, $C_p(\mathbf{r})\to\delta(\mathbf{r})$. In the case $D_2=2$ one arrives at typical dependence $S_p(k)\propto k^{-2}$ for diffuse spreading on the structured (let us say flat) surface. Here, the topological dimension d equals the fractal dimension D_2. Therefore, a variation of the fractal dimension D_2 versus the time indicates a change in the fractal morphology of the surface from pure uncorrelated Gaussian surface toward well-structured surface having fractal dimension $d=D_2=2$.

In order to study scaling properties of the system under consideration we will compare all our results obtained with results coming from an investigation of the anisotropic system with additive fluctuations. As a reference system we consider the model described by the Langevin equation with additive noise, i.e., $\partial_t h=\nu_\alpha\nabla^2_{\alpha\alpha}h+(\Lambda_\alpha/2)(\nabla_\alpha h)^2-K\nabla^2(\nabla^2 h)+\zeta(\mathbf{r},t)$, where ζ is the Gaussian random source with properties $\langle\zeta\rangle=0$ and $\langle\zeta(\mathbf{r},t)\zeta(\mathbf{r}',t')\rangle=2\Sigma\delta(\mathbf{r}-\mathbf{r}')\delta(t-t')$. Calculations of the dynamical exponents at the system parameters $a_\sigma=1.2$, $\theta=0.4$, $F=1.0$, $\sigma=1.0$, $K=2.0$, $\Sigma=1.0$, and $r_c=1.0$ are shown in Fig. 5.

According to the scaling hypothesis the temporal evolution of the quantity $W^2=\langle(\delta h)^2\rangle$, where $\delta h=h-\langle h\rangle$, can be represented through the exponent β as $\langle(\delta h)^2\rangle\propto t^{2\beta}$. In a short-time limit it was found experimentally that the exponent β varies in the interval 0.1–2.9 (see, for example, Ref. [38] and citations therein). It was shown that its magnitude depends on the properties of the target material, ion type, ion energy, and angle of incidence. In Ref. [6] numerical estimation of the growth exponent β was performed for the isotropic Kuramoto-Sivashinsky equation with $\nu_x=\nu_y=-0.2$, $\Lambda_x=\Lambda_y=1.0$, and $K=2.0$ with additive fluctuations of the uniform distribution. It was shown that the quantity β depends on the time and varies in the interval 0.22–0.7 during the system evolution. We have computed the growth exponent for such kind of the isotropic system parameters with additive noise having Gaussian distribution and found that at small time interval $t\leq 10$ the exponent $\beta\simeq 0.25$; at large time limits $t\leq 100$ one has $\beta\simeq 0.8$ (see empty squares in Fig. 5) [42]. Such time dependence means that at early stages where growth processes are realized there is a straight line for $W^2(t)$ in a log-log plot. At large-time limit where coarsening processes start to play essential role there is a set of exponents $\{\beta_i\}$. Such set means that one can use the local power-law approximation for the smooth function $W^2(t)$ where each exponent β_i relates to the fixed time interval Δt_i: $W^2(\Delta t_i)\propto(\Delta t_i)^{2\beta_i}$. According to such assumption the function $\phi(\cdot)$ in Eq. (15) should behave itself in a more complicated form on a given time interval Δt_i than the simplest power law shown above. The proposed approximation allows one to study at what time interval nonlinear effects are responsible for the system evolution.

It is interesting to note that for the anisotropic system with additive Gaussian noise the growth exponent takes values more than 1 versus evolution time (see black squares in Fig. 5). At early stages (growth processes) one has $\beta\simeq 0.29$, and we arrive at results well related to experimental observations of growth processes at ion-beam sputtering (see Refs. [39,40]). During the system evolution β grows faster than it was for isotropic system and exceeds 1. It means that the coarsening processes in anisotropic system occur faster than in the isotropic one. It is seen from the inset of the interface width $W^2(t)$ in Fig. 5.

Comparing values for the roughness exponent α for both isotropic and anisotropic systems one can see that in anisotropic system the quantity α takes elevated values (cf. empty and black circles in Fig. 5). It is well known that in anisotropic systems there are two kinds of roughness exponents related to parallel and perpendicular beam directions; such exponents can exceed the value of 1 [41]. In our study we consider the integral effect and do not distinguish such kind of roughness exponents. The time dependence of the roughness exponent can be considered as a set of exponents $\{\alpha_i\}$, meaning that the function $\psi(\cdot)$ in Eq. (17) has more complicated dependence in a local time interval than its simplest power-law version.

Let us consider the anisotropic system with multiplicative fluctuations. As it was before, we use power-law approximations for the local change of the smooth correlation function $C_h(\mathbf{r},t)$ to compute sets $\{\beta_i\}$ and $\{\alpha_i\}$. We have performed calculations of the scaling exponents at the fixed point in the

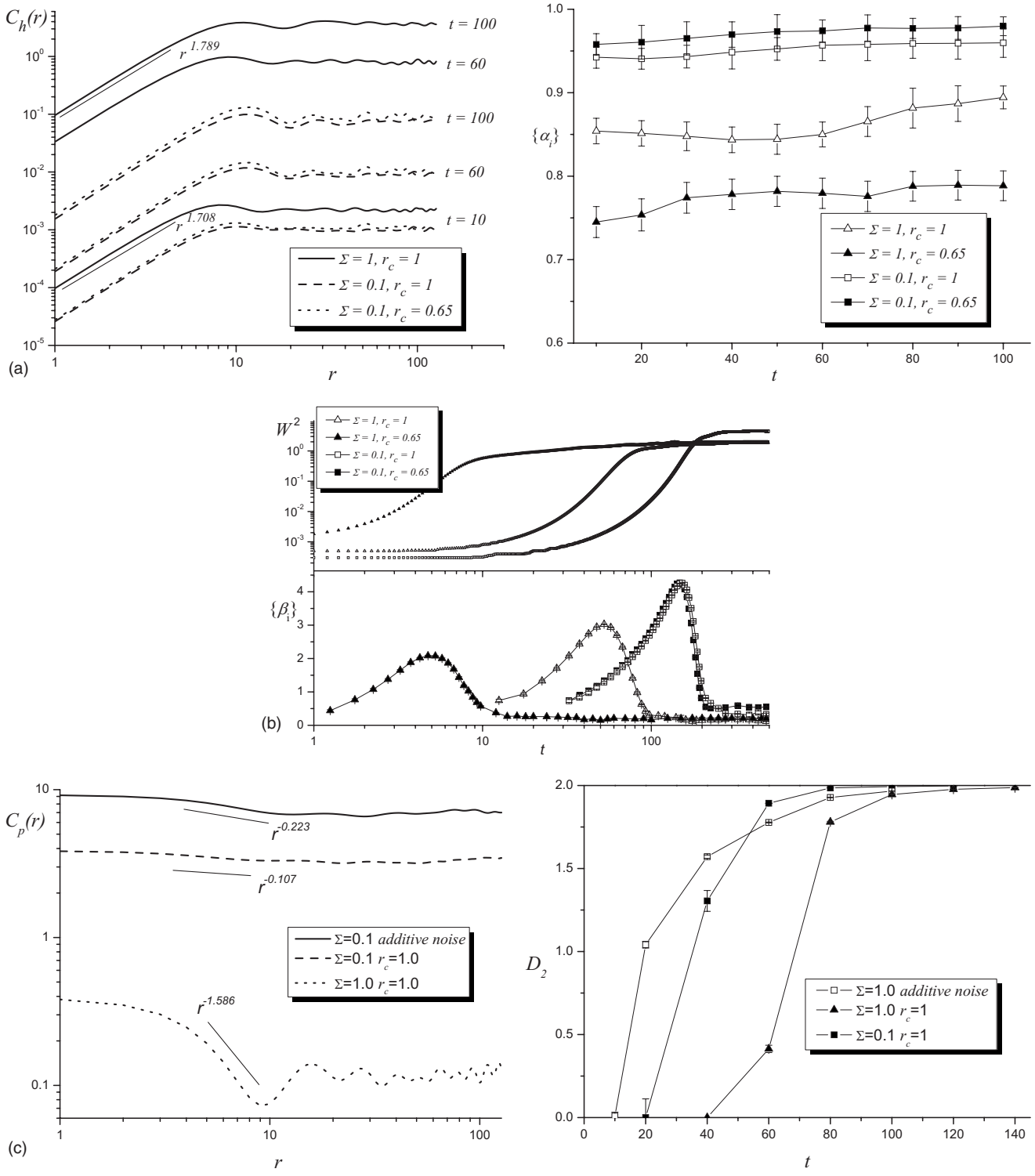

FIG. 6. (a) The correlation function $C_h(r)$ and the roughness exponent α versus time. (b) The interface width W^2 versus time. (c) The correlation function $C_p(r)$ at t=60 and the fractal dimension D_2 versus time. Other parameters are a_σ=1.2, θ=0.4, F=1, σ=1, and K=2.

phase diagram (θ, a_σ) at different values of the noise intensity Σ and the correlation radius r_c. The reference point is a_σ=1.2, θ=0.4, F=1.0, σ=1.0, K=2.0 (point 1 in the phase diagram in Fig. 4). We compute α_i and β_i at time window when the interface width W or the correlation function $C_h(r)$ starts to grow until they saturate.

The corresponding dependencies of $\{\alpha_i\}$, $\{\beta_i\}$, and D_2 are shown in Fig. 6. In Fig. 6(a) we plot the correlation function $C_h(r;t)$ and the roughness exponents $\{\alpha_i\}$, Fig. 6(b) illustrates the time dependence of the interface width $W^2(t)$, and Fig. 6(c) shows the pair-correlation function $C_p(r;t)$ and the associated fractal dimension D_2 at fixed times. From Fig.

6(a) it follows that the growth process is nonstationary for early stages and the roughness exponents are near 0.95 for small angle of incidence dispersion Σ. At such set of the control parameters (a_σ and θ) and small Σ the correlation radius r_c has no essential influences on the system behavior. At large Σ the roughness exponent has lower magnitudes and exponents $\{\alpha_i\}$ have different values at different time intervals. At small r_c and large Σ the values for the roughness exponent decrease.

Let us consider the system behavior at small times, where growth and coarsening processes are realized. Comparing curves for the interface width at different Σ's and r_c's on one hand and the growth exponent dependencies versus time on the other one [see Fig. 6(b)], one can conclude that as the noise intensity Σ increases the position of the peak of the exponent β reduces to small time. It means that as the noise intensity increases at such choice of the control parameters the interface width grows at smaller time interval than at low Σ. Alternatively, the shift of the peak position at large Σ indicates that multiplicative fluctuations are responsible for nonlinear effects appearing at small times. It looks natural due to the nonlinear form of the multiplicative noise, where the large noise contribution influences crucially properties of the growth processes. From the physical viewpoint it means that large fluctuations promote fast growth processes (in a short time interval with small $\beta_i < 1$) and the coarsening processes occur with $\beta_i \lesssim 3$. At small noise intensity growth processes are delayed in time (occur later than at large Σ), while coarsening ones are accelerated with $\beta_i \lesssim 4$. Therefore, the multiplicative noise in anisotropic systems is able to accelerate growth and coarsening processes on one hand. On the other one it is responsible for decreasing the time interval where these processes are realized. The correlation properties of fluctuations characterized by r_c have no crucial influence on the growth processes at small noise intensities. At large Σ small values for the correlation scale r_c reduce magnitudes for the growth exponent; growth and coarsening processes occur earlier than at large r_c. At large time intervals where the true scaling regime is observed there is no essential difference in values β_i at different time windows. Here, as the noise intensity increases the values for β_i decrease (cf. black triangles and squares); variations in correlation radius do not lead to change in β_i (cf. empty and black triangles). In next study we shall focus our attention on growth and coarsening processes which are realized at small time intervals.

A change in the fractal properties of the surface is shown in Fig. 6(c). Here, we compare fractal properties of two different systems, namely, that with additive fluctuation source and that with multiplicative noise. From the dependencies of the pair-correlation function $C_p(r)$ it is seen that at $t=60$ the additive noise contribution leads to a picture when the correlation function $C_p(r)$ decreases slowly with exponent $\Delta=0.227$, whereas the multiplicative noise contribution with the same intensity $\Sigma=1.0$ at $r_c=1.0$ increases the exponent Δ to 1.587. According to the definition of the correlation dimension D_2 it means that the fractal properties of the surface is well pronounced at multiplicative noise with large intensity at a small time interval $t \simeq 60$ [see curve $D_2(t)$]. From the time dependencies of the fractal dimension D_2 for the system with multiplicative noise it follows that at small times the surface has Gaussian properties of the kind of white noise in space (the correlation function has the from of the Dirac delta function.). At small time interval (at intermediate times) the fractal properties emerge and characterized by $0 < D_2 < 2$. At large times one has $D_2=2$ and the well-structured patterns are observed; its dimension D_2 coincides with the topological $d=2$. In the case of additive fluctuations the time interval of the formation of well-structured patterns is larger than in system with multiplicative noise.

Next let us compare the time dependencies for the scaling exponents for different sets of the system parameters a_σ and θ shown in Figs. 7(a) and 7(b). It is seen that at $a_\sigma=2.0$ and $\theta=0.4$ [Fig. 7(a)] the behavior of the system is the same as it was in the previous case. Here, at large noise intensity maximal magnitude of β_i is smaller and is observed earlier than at small noise intensity. With a decrease in r_c at large Σ the set of growth exponents is observed at earliest time interval. Moreover, small correlation radius of fluctuations decreases maximal β_i. These results look natural due to the points with coordinates $a_\sigma=1.2$, $\theta=0.4$ and $a_\sigma=2.0$, $\theta=0.4$ (points 1 and 2 in Fig. 4) that belong to one domain of the phase diagram. Variations in r_c have no essential influence on the system dynamics and roughness of the surface at small Σ. Comparing curves for the fractal dimension D_2 for above two sets of the system parameters one can see that at small Σ the quantity D_2 is less than that in the previous case [cf. dependencies $D_2(t)$ in Figs. 6(c) and 7(a)].

In Fig. 7(b) we consider dynamics of the systems in another domain of the phase diagram shown in Fig. 4 (vicinity of point 3). Here, at small Σ the universal law for growth processes can be realized earlier than at large fluctuations. Moreover, large noise intensity delays dynamics of the system evolution. A decrease in β_i and α_i at large Σ relates to the morphology change shown in the corresponding snapshots. It means that the phase diagram shown in Fig. 4 will be modified under variation of Σ. Here, the quantity r_c does not change values for α_i and β_i at small Σ and cannot lead to the morphology change of the surface. At large fluctuation intensity and small correlation scale the dynamics of the system is the same as that at large r_c, but all processes occur earlier at small r_c. As in previous cases large Σ and small r_c provide a decrease in the roughness exponent values.

Figure 8 shows the evolution of the spherically averaged structure function defined on a circle,

$$S_h(k,t) = \frac{1}{N_k} \sum_{k \le \mathbf{k} \le k+\Delta k} S_h(\mathbf{k},t), \tag{21}$$

where N_k is the number of points on the circle of width Δk. Two different choices of the noise intensity Σ and the correlation radius of fluctuations r_c are shown in Figs. 8(a)–8(c), respectively. It is seen that during the system evolution at early stages the system selects the ripples with the corresponding wave number (dotted lines), and after at late stages the algebraic form for the structure function is realized. At large time intervals one can define the exponent α from the definition $S_h(k) \propto k^{-(d+2\alpha)}$. As shown in Figs. 8(a) and 8(b) for the above system parameters one has $S_h(k) \propto k^{-3.86}$ for $\Sigma=0.1$ and $S_h(k) \propto k^{-3.92}$ for $\Sigma=1.0$, where $d=2$. Hence, the

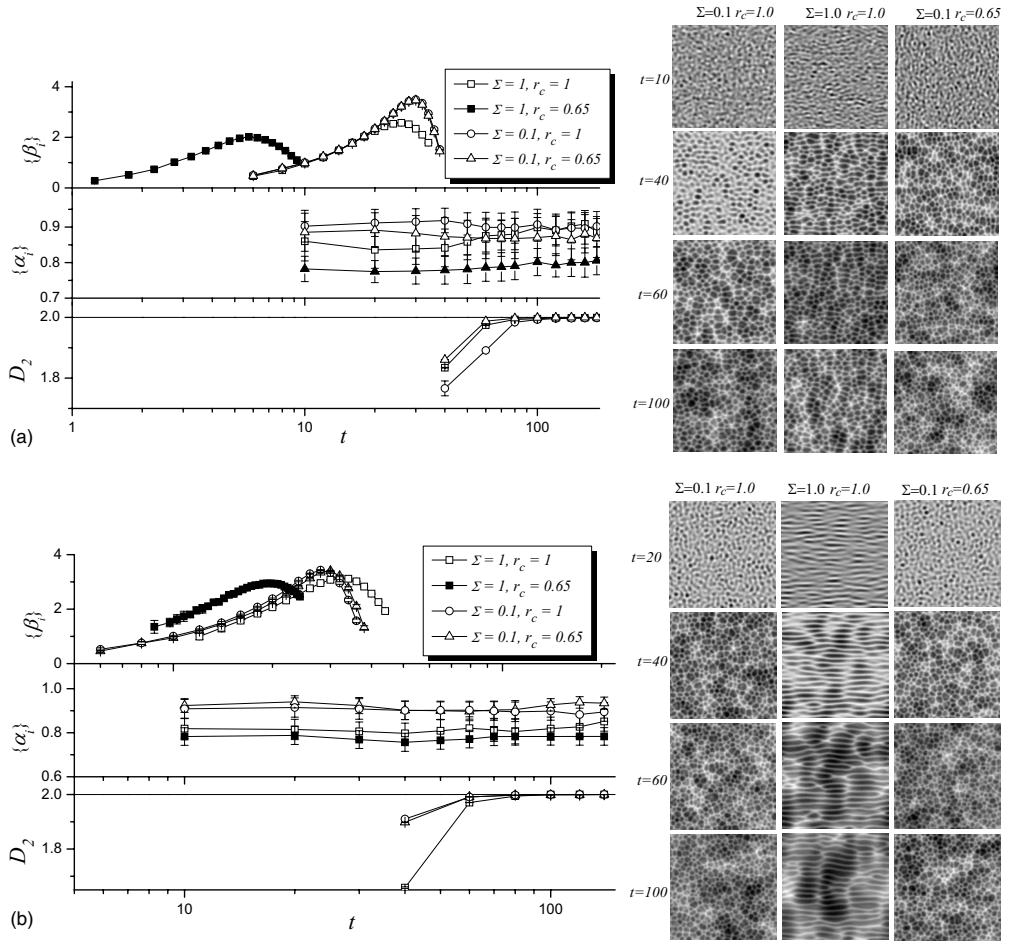

FIG. 7. Scaling exponents α and β and correlation dimension D_2 versus time at (a) a_σ=2.0, θ=0.4 (point 2 in the phase diagram in Fig. 4) and (b) a_σ=2.0, θ=0.2 (point 3 in the phase diagram in Fig. 4). Typical snapshots of the system evolution are taken at different Σ's and r_c's. Other parameters are F=1, σ=1, and K=2.

roughness exponent takes values $\alpha \simeq 0.93$ and $\alpha \simeq 0.96$ that are well predicted by the analysis of the correlation function $C_h(r)$ [see Fig. 6(a)].

V. CONCLUSIONS

We have studied the ripple formation processes induced by the ion sputtering under stochastic conditions of illumination. The main assumption was the stochastic nature of the ion beam when the angle of incidence is distributed in space and time (homogeneous and stationary field). It allows us to generalize the Bradley-Harper model of ripple formation [3] and consider the stochastic model with multiplicative fluctuations describing the random nature of the incidence angle proposed in Ref. [9]. We have discussed properties

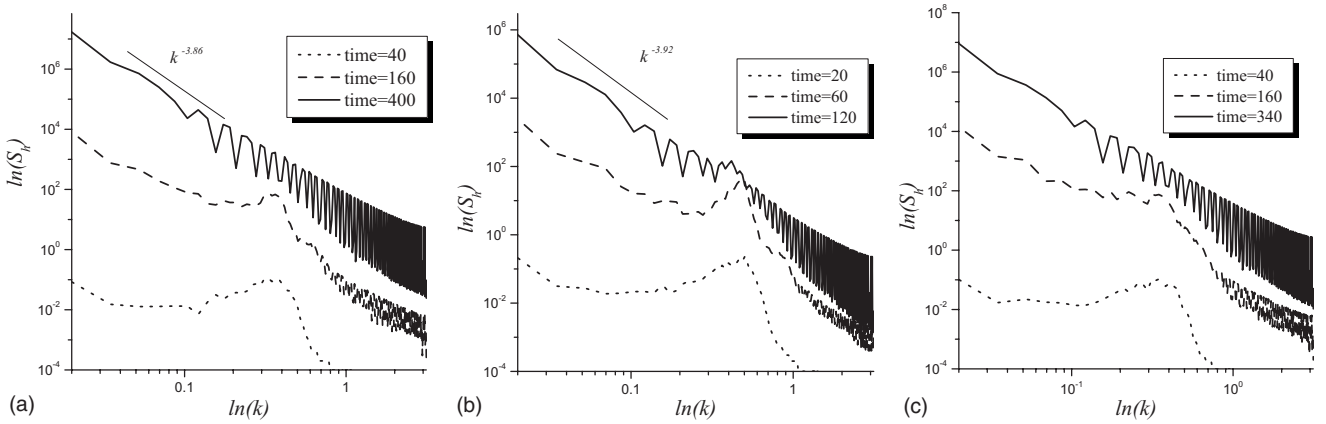

FIG. 8. Evolution of the spherically averaged structure function $S_h(k,t)$ at different noise intensities: (a) Σ=0.1, r_c=1; (b) Σ=1.0, r_c=1; (c) Σ=0.1, r_c=0.65. Other parameters are a_σ=1.2, θ=0.4, F=1, and σ=1.

of the ripple formation in both linear and nonlinear models.

Within the framework of the linear stability analysis we have shown that even in the linear system the noise action is able to change the critical values for the control parameters of the system such as the penetration depth and the averaged incidence angle. It was found that as correlation properties of such multiplicative noise the dispersion in the incidence angles around the average can reduce the domains of the control parameters where the ripples change their orientation at the fixed angle of incidence.

Studying the nonlinear model we have computed the dynamic phase diagram illustrating the formation of different patterns (ripples and holes), which relates to the results from the linear stability analysis. Main properties of the ripple formation were studied with the help of the distribution function of the height and its averages reduced to the skewness, kurtosis, and interface width (dispersion). To make a detailed analysis of the ripple formation we have examined the scaling behavior of main statistical characteristics of the system reduced to the correlation functions and its Fourier transforms (structure functions). It was shown that the growth and roughness exponents depend on the control parameters (it was predicted by previous study of the isotropic Kuramoto-Sivashinsky equation [6]); these exponents depend on the noise intensity. Comparing results for the system with additive and multiplicative fluctuations it was shown that multiplicative noise can crucially accelerate processes of ripple formation, increasing the growth exponent. As long as our system is anisotropic the noise action is different at different sets of the main control parameter values. Studying fractal properties of the surface we have calculated the fractal (correlation) dimension as the time-dependent function. It was shown that in the system with multiplicative noise the fractal properties appear at small time interval of the surface growth, whereas in the system with the additive noise this time interval is wider. These results are well predicted by the correlation functions analysis and by Fourier transformation of the numerically calculated surface.

Therefore, as patterning, the scaling behavior of the system can be controlled by additional set of parameters reduced to the dispersion of the angle of incidence and the correlation properties of its fluctuations. As fluctuation intensity increases growth and coarsening processes occur earlier. The same situation is observed when the correlation scale decreases.

[1] L. Jacak, P. Hawrylak, and A. Wojs, *Quantum Dots* (Springer-Verlag, Berlin, 1998).

[2] M. Navez, C. Sella, and D. Chaperot, *Ionic Bombardment: Theory and Applications*, edited by J. J. Trillat (Gordon and Breach, New York, 1964).

[3] R. M. Bradley and J. M. E. Harper, J. Vac. Sci. Technol. A **6**, 2390 (1988).

[4] R. Cuerno and A.-L. Barabasi, Phys. Rev. Lett. **74**, 4746 (1995).

[5] M. Makeev and A.-L. Barabasi, Appl. Phys. Lett. **71**, 2800 (1997).

[6] J. T. Drotar, Y.-P. Zhao, T.-M. Lu, and G.-C. Wang, Phys. Rev. E **59**, 177 (1999).

[7] T. Aste and U. Valbusa, Physica A **332**, 548 (2004).

[8] B. Kahng and J. Kim, Curr. Appl. Phys. **4**, 115 (2004).

[9] R. Kree, T. Yasseri, and A. K. Hartmann, Nucl. Instrum. Methods Phys. Res. B **267**, 1407 (2009).

[10] S. Rusponi, C. Boragno, and U. Valbusa, Phys. Rev. Lett. **78**, 2795 (1997).

[11] S. Rusponi, G. Costantini, C. Boragno, and U. Valbusa, Phys. Rev. Lett. **81**, 2735 (1998).

[12] E. Chason *et al.*, Phys. Rev. Lett. **72**, 3040 (1994).

[13] J. Erlebacher, M. J. Aziz, E. Chason, M. B. Sinclair, and J. A. Floro, Phys. Rev. Lett. **82**, 2330 (1999).

[14] W.-Q. Li *et al.*, Appl. Surf. Sci. **252**, 7794 (2006).

[15] W. J. Moberly Chan *et al.*, MRS Bull. **32**, 424 (2007).

[16] H. X. Qian *et al.*, Appl. Surf. Sci. **240**, 140 (2005).

[17] D. Paramanik *et al.*, J. Nanosci. Nanotechnol. **8**, 4207 (2008).

[18] J. Lian *et al.*, Appl. Phys. Lett. **88**, 093112 (2006).

[19] S. Facsko *et al.*, Science **285**, 1551 (1999).

[20] M. Kardar, G. Parisi, and Y.-C. Zhang, Phys. Rev. Lett. **56**, 889 (1986).

[21] D. E. Wolf and J. Villian, EPL **13**, 389 (1990).

[22] Y. Kuramoto and T. Tsuzuki, Prog. Theor. Phys. **55**, 356 (1976); G. I. Sivashinsky, Acta Astronaut. **6**, 569 (1979).

[23] B. Ziberi *et al.*, Appl. Phys. Lett. **92**, 063102 (2008).

[24] P. Sigmund, J. Mater. Sci. **8**, 1545 (1973).

[25] M. A. Makeev and A.-L. Barabasi, Nucl. Instrum. Methods Phys. Res. B **222**, 316 (2004).

[26] J. W. Cahn and J. E. Taylor, Acta Metall. Mater. **42**, 1045 (1994).

[27] P. Sigmund, Phys. Rev. **184**, 383 (1969).

[28] C. W. Gardiner, *Handbook of Stochastic Methods* (Springer-Verlag, Berlin, 1985).

[29] J. Garcia-Ojalvo and J. M. Sancho, *Noise in Spatially Extended Systems* (Springer, New York, 1999).

[30] E. A. Novikov, Zh. Eksp. Teor. Fiz. **47**, 1919 (1964) [Sov. Phys. JETP **20**, 1290 (1965)].

[31] J. M. Sancho, M. San Miguel, S. L. Katz, and J. D. Gunton, Phys. Rev. A **26**, 1589 (1982); M. S. Miguel and R. Toral, arXiv:cond-mat/9707147, *Instabilities and Nonequilibrium Structures VI*, edited by E. Tirapegui and W. Zeller (Kluwer Academic) (2000).

[32] G. E. P. Box and Mervin E. Muller, Ann. Math. Stat. **29**, 610 (1958).

[33] C. H. Lam and F. G. Shin, Phys. Rev. E **57**, 6506 (1998).

[34] L. Giada, A. Giacometti, and M. Rossi, Phys. Rev. E **65**, 036134 (2002).

[35] F. Family and T. Vicsek, J. Phys. A **18**, L75 (1985).

[36] F. Family, Physica A **168**, 561 (1990).

[37] S. K. Sinha, E. B. Sirota, S. Garoff, and H. B. Stanley, Phys. Rev. B **38**, 2297 (1988).

[38] Maxim Makeev, Rodolfo Cuerno, and Albert-Laszlo Barabasi, Nucl. Instrum. Methods Phys. Res. B **197**, 185 (2002).

[39] X.-S. Wang, R. J. Pechman, and J. H. Weaver, J. Vac. Sci. Technol. B **13**, 2031 (1995).

[40] E. Chason and T. M. Mayer, Appl. Phys. Lett. **62**, 363 (1993).
[41] Adrian Keller, Rodolfo Cuerno, Stefan Facsko, and Wolfhard Moller, Phys. Rev. B **79**, 115437 (2009).
[42] The difference between values for β in Ref. [6] and in our study can be proved by different models for the additive noise term (we use Gaussian distributed random numbers, while authors of Ref. [6] have used random numbers with uniform distribution).